Environmental Science & Technology

pubs.acs.org/est

Article

First Insight into the Mobilization and Sequestration of Arsenic in a Karstic Soil during Redox Changes

Jianxu Wang,* Sabry M. Shaheen, Ann-Christin Swertz, Chengshuai Liu, Christopher W.N. Anderson, Scott Fendorf, Shan-Li Wang, Xinbin Feng, and Jörg Rinklebe*

Cite This: *Environ. Sci. Technol.* 2024, 58, 17850−17861

Read Online

ACCESS | Metrics & More | Article Recommendations | Supporting Information

ABSTRACT: Karst terrains provide drinking water for about 25% of the people on our planet, particularly in the southwest of China. Pollutants such as arsenic (As) in the soil can infiltrate groundwater through sinkholes and bedrock fractures in karst terrains. Despite this, the underlying mechanisms responsible for As release from karst soils under redox changes remain largely unexplored. Here, we used multiple synchrotron-based spectroscopic analyses to explore As mobilization and sequestration in As-polluted karstic soil under biogeochemical conditions that mimic field-validated redox conditions. We observed that As in the soil exists primarily as As(V), which is mainly associated with Fe(oxyhydr)oxides. The concentration of the dissolved As was high (294 μM) and As(III) was dominant (~95%) at low E_h (≤−100 mV), indicating the high risk of As leaching under reducing conditions. This As mobilization was attributed to the fact that the dissolution of ferrihydrite and calcite promoted the release and reduction of associated As(V). The concentration of the dissolved As was low (17.0 μM) and As(V) was dominant (~68%) at high E_h (≥+100 mV), which might be due to the oxidation and/or sequestration of As(III) by the recrystallized ferric phase. Our results showed that the combined effects of the reductive release of As(V) from both ferric and nonferric phases, along with the recrystallization of the ferric phase, govern the redox-induced mobilization and potential leaching of As in soils within karst environments.

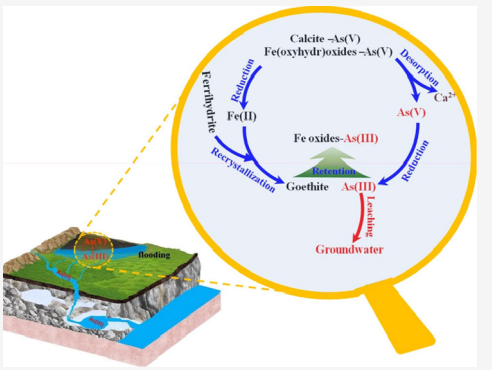

KEYWORDS: *arsenic mobilization, reducing-oxidation reactions, dissimilatory reduction, biogeochemical microcosms*

INTRODUCTION

Karst regions are globally distributed and supply drinking water to approximately 25% of the population.[1] In China, carbonate rocks cover an area of approximately 3.44 × 10^6 km^2, accounting for 33% of the total land area. The majority of the karst landscapes are concentrated in the southwestern part of the country. This distribution coincides with numerous ore deposits containing toxic elements such as arsenic (As), cadmium (Cd), and mercury (Hg) due to low-temperature metallogenesis.[2] Arsenic contamination, in particular, is a major concern, with over 61% of Chinese As resources (2.5 million tons) being distributed in southwestern China. This accounts for 42% of the globally explored reserves. Anthropogenic and natural activities have resulted in the dispersion of As throughout the karst regions, sparking concerns about potential groundwater contamination with As.

The concentration of As in karstic soil has been documented as exceedingly high, reaching concentrations as high as 4000 mg kg^{-1}.[3] Karstic soil is characterized by its high pH and carbonate content, as well as a thin soil profile.[4,5] These characteristics can limit the natural filtering effect of the soil on As. This is due to competition between carbonate and As oxyanions for binding with Fe(oxyhydr)oxides. Additionally, the alkaline pH supports desorption of As oxyanions, further reducing the filtering effect.[6] Frequent flooding and rising water tables caused by climate change also trigger biogeochemical processes that release As from the soil/sediment into groundwater. Arsenic leaching from soils is a significant contributor to contamination of both surface and underground aquifers in karst regions. However, despite the well-documented As contamination of aquifers in karst regions, the biogeochemical processes that control As mobilization within these environments remain poorly understood.[7]

Arsenic is redox-sensitive, and thus its release and mobilization in soils are mainly governed by the changes of redox potential (E_h). The dominant mechanisms underlying the redox-induced (im)-mobilization of As in soils include microbial-mediated reductive dissolution of Fe(oxyhydr)-oxides, oxidative dissolution of As-rich sulfide minerals, and

Received: March 25, 2024
Revised: September 12, 2024
Accepted: September 13, 2024
Published: September 25, 2024

https://doi.org/10.1021/acs.est.4c02989
Environ. Sci. Technol. 2024, 58, 17850−17861

competitive adsorption of anions HCO_3^- and PO_4^{3-}.[8,9] Under anaerobic conditions, microbial respiration plays a pivotal role in regulating dissolution of Fe(oxyhydr)oxides.[10] Microbes such as dissimilatory As(V)-respiring prokaryotes (DARPs), *Shewanella oneidensis* MR-1, and *Sulfurospirillum barnesii*, which possess As(V) respiratory reduction genes (*Arr*), facilitate the reduction of As(V) and Fe(III).[11−13] In the models of DARP-mediated As(V) reduction, bacteria facilitate the mobilization of As(V) from mineral surfaces by conversion to As(III). The primary mechanism that facilitates the immobilization of As(V) and As(III) in soils involves their adsorption onto Fe(oxyhydr)oxides. Under aerobic conditions, the oxidation of As(III) to As(V), followed by its adsorption on and/or (co)-precipitation with Fe(oxyhydr)oxides, results in a marked immobilization of As.[14] Arsenic (im)mobilization processes in soils are also modulated by various factors such as δ-MnO_2, aluminum oxides, organic matter, sulfide, (bio)carbonate, and calcite. The presence of δ-MnO_2 can promote the oxidation and immobilization of goethite-adsorbed As because goethite particles are distributed on the δ-MnO_2 surface, which supports As(III) oxidation by δ-MnO_2.[15] In the absence of Fe(oxyhydr)oxides, As(V) adsorption onto the surface of aluminum oxides forms aluminum As(V)-like precipitate.[16] However, in the aluminum-Fe(oxyhydr)oxide environment, the mobilization of As is strongly dependent on bacterial function. For example, in the presence of As(V) reducing bacteria (*Citrobacter* sp. JH012-1), Al promoted the release of As by affecting the distribution of As(III) and As(V) between the solid and aqueous phases.[17] Dissolved organic matter (DOM) can promote the reductive dissolution of Fe-(oxyhydr)oxides, subsequently releasing As bound to Fe-(oxyhydr)oxides. Solaiman et al.[18] reported that a lower carbon:nitrogen ratio of DOM was favorable for the mobilization of As. Excessive sulfide can hinder the adsorption of As(III) onto Fe(oxyhydr)oxides by forming As_2S_3.[19] Additionally, biocarbonate can react with arsenian pyrite and As_2S_3, leading to the formation of arseno-carbonate complexes,[6,20] which compete with As(V)/As(III) for adsorption sites on Fe(oxyhydr)oxides.[21] In scenarios where Fe(oxyhydr)-oxides are scarce, As may be adsorbed onto calcite or integrated into the crystal lattice of carbonate minerals,[22] with As(V) exhibiting a preferential sorption over As(III) in the natural environment.[23] Furthermore, carbonate and its complexes can occupy the surface area of Fe(oxyhydr)oxides, thus inhibiting their reductive dissolution and the ability to absorb As.[24−26] Regarding pH, high pH favors the adsorption of As(III) onto Fe(oxyhydr)oxides, and this adsorption remains pH-independent within a range of 4.0−8.0,[27] whereas low pH favors the adsorption of As(V) onto Fe(oxyhydr)-oxides (e.g., goethite and gibbsite).[28] As for anions, Yi et al.[9] reported that the competitive adsorption of phosphate resulted in the increased concentration of As(V) in the shallow groundwater.

Despite numerous studies on the mobilization of As in soils, the redox-induced dynamics of As in naturally contaminated karstic soil remains unclear. Furthermore, the widespread conversion of upland soils into paddy fields, driven by the demand for rice production stemming from population growth, along with the consequent alterations in redox conditions and biogeochemical factors, has the potential to impact the biogeochemical cycle and release of As in soils.[29] However, the precise extent of this impact on As behavior is yet unknown. To address this knowledge gap, we examined the biogeochemical processes that govern As fate in an As-polluted karstic soil across varying E_h. This knowledge will enhance our ability to predict As leaching risks from soils prone to frequent flooding under the scenario of climate change and aid in developing strategies for managing As-polluted soils in karstic regions globally.

MATERIALS AND METHODS

Description of Sampling Site. The soil sampling site is located at the Laowanchang gold mining site within a typical karst environment in Qinglong County, Guizhou province, China, where rocky desertification accounts for almost 41% of the total land area.[30] The region contains abundant carbonate rocks with an annual precipitation of 1532 mm.[31] All of these topographical characteristics are favorable for the leaching of contaminants. The Laowanchang gold mine is a Carlin-type gold deposit, characterized by Au−As−Hg−Sb−Tl mineralization. Arsenic is present in soils at a concentration of up to 4000 mg kg^{-1}, and leaching from soil is reported to be the important pathway of groundwater contamination by As.[3] Monitoring work has recorded an As concentration 100 times greater in groundwater connected to mineralization relative to a control site in Qinlong County.[31]

Soil Collection and Characterization. A composite surface soil sample (0−15 cm) was randomly collected from a contaminated site at the Laowanchang gold mining site. Soil samples were air-dried, crushed, and sieved for the biogeochemical microcosm study. Soil pH and organic matter content were determined using standard methods.[32] Soil carbonate content was quantified using a carbonate detector (Eijkelkamp Agrisearch Equipment, The Netherlands). Subsamples were digested with *aqua regia* in a microwave system (Milestone MLS 1200 Mega, Germany), and the digest solutions were analyzed for S, calcium (Ca), Fe, manganese (Mn), and As concentrations using ICP-OES. Water-soluble As was extracted according to the method of Wang et al.[3] Total CaO, Al_2O_3, Na_2O, K_2O, MgO, and SiO_2 in the original soil were determined with an X-ray fluorescence spectrometer (AxiosmAX, PANalytical B.V., The Netherlands). The general physicochemical properties of the soil are provided in the Supporting Information, Table S1. The distribution of As, Ca, and Fe, the As valence state, and the mineralogical phase of the original soil particles were investigated using synchrotron-based X-ray fluorescence spectroscopy (μ-XRF), micro-X-ray absorption near-edge structure (μ-XANES) spectroscopy, and micro-X-ray diffraction (μ-XRD) at the 4-BM XFM beamline of NSLS II. The analytical details and processing of spectral data have been published elsewhere and are presented in the Supporting Information, S1.1.[33,34] For TEM-EDS analysis, the original soil powders were dispersed with 50% ethanol, mounted in a carbon-covered copper grid, and analyzed using an analytical transmission electron microscope (Tecnai G2 F20 S-TWIN TMP, FEI Co., America) coupled with energy-dispersive X-ray (EDX) spectroscopy.

Biogeochemical Microcosm Experiment. We used a well-developed biogeochemical microcosm system (MC) to simulate the varied redox potential (E_h) conditions of soil. This system includes a stirrer, an E_h-platinum (Pt) electrode, a pH electrode, and a thermometer, and it is capable of simulating oxic or anoxic environments by flushing with synthetic air/O_2 or N_2. The details of the calibration and measurement of pH, E_h, and temperature sensors are presented in the Supporting Information, S1.2. A portion of 210 g of air-dried soil and 1680

https://doi.org/10.1021/acs.est.4c02989
Environ. Sci. Technol. 2024, 58, 17850−17861

mL of water were added to each MC. The concentration of water-soluble As in the soil was 9.2 μM, which set as a base for the dissolved concentration of As in the original soil before changing of E_h and its induced potential changes in soil pH, governing factors, and therefore the mobilization of As. Approximately 15 g of powdered wheat straw and 10 g of glucose were introduced into each MC to provide carbon sources for microorganisms, thereby eliminating any potential carbon-limitation effect. Glucose, being highly bioavailable, can be rapidly utilized by microorganisms, providing an immediate carbon source. Conversely, wheat straw, though less bioavailable than glucose, serves as a long-term carbon source for microbial communities. The details of the system have been published elsewhere.[35]

The lowest E_h value (close to −350 mV) was achieved after 65 h of reaction as a result of anaerobic microbial metabolism (Figure S1). The E_h was then raised sequentially in 100 ± 20 mV increments by flushing with synthetic air (N_2/O_2, 79.5/20.5 vol %) or O_2. Once target E_h values were attained, the system was flushed with N_2 or synthetic air to maintain each E_h window for about 48 h, after which time a soil suspension sample was taken. In total, seven preset E_h windows (treatments), including −300, −200, −100, 0, + 100, + 200, and +300 mV, were set and sampled, and three independent MC replicates were used for each treatment. The E_h and pH data for each MC were logged every 10 min during the experiment. The actual E_h ranged from about −350 to +310 mV (Figure S1), which covers E_h ranges recorded in the environment.[36,37] The pH−E_h plots for the three replicated MCs are shown in Figure S1.

At sampling, about 80 mL of soil suspension collected from each MC was transferred into two 50 mL centrifuge tubes in an anaerobic glovebox under a 95% N_2/5% H_2 atmosphere (A35 anaerobic workstation, Don Whitley Scientific Limited, UK). All soil suspensions were centrifuged at 5000 rpm for 10 min. About 40 mL of supernatant was filtered through a 0.45 μm pore-size membrane (Whatman, Inc.) in the anaerobic glovebox to obtain the dissolved fraction (liquid phase).[38] The liquid phase sample was divided into five subgroups for total dissolved As, As speciation (As(III) and As(V)), total dissolved Fe, dissolved organic carbon (DOC), and sulfate analyses. Subsamples for As and Fe analysis were acidified to 2% by using trace metal-grade HNO_3 prior to analysis.

The residual supernatant was filtered through an 8 μm pore-size membrane in the anaerobic glovebox, and thereafter it was subjected to ultracentrifugation at 14,000 g for 1 h (CS150GXII, Hitachi, Ltd., Japan) to obtain the colloid fraction (colloidal phase).[39]

The remaining soil solid samples after centrifugation and filtration collected from triplicate MCs at each targeted E_h window were mixed to generate one composite soil sample (soil solid phase). Each composite was further divided into four subgroups to determine the microbial community composition, as well as As, sulfur (S), and iron (Fe) speciation.

Liquid Sample Analysis. DOC was analyzed using a C/N analyzer (Analytik Jena, Jena, Germany), and sulfate was measured using an ion chromatograph (Personal IC 790, Metrohm, Filderstadt, Germany). Total As and Fe concentrations were analyzed by inductively coupled plasma-optical emission spectroscopy (ICP-OES) (Ultima 2, Horiba JobinYvon, Unterhaching, Germany), with As(III) and As(V) concentrations determined using HPLC-ICP-MS.[40]

Soil Sample Analysis. Morphology and chemical compositions of the colloidal phase were characterized with a scanning transmission electron microscope (STEM, Hitachi HD-2700, Hitachi High-Technologies Corp., Tokyo, Japan) using the standard method.[41]

The solid phase of soil samples from E_h windows of −300, −200, 0, + 300 mV, and the original soil were analyzed for As, Fe, and S speciation. Samples were freeze-dried and mounted onto sample holders by Kapton tape in an anaerobic glovebox and analyzed for As K-edge XANES and Fe K-edge XANES at beamline 07 A and beamline 17C, respectively, at the National Synchrotron Radiation Research Center (NSRRC), Hsinchu, Taiwan, ROC. Sulfur speciation was analyzed at beamline 4B7A at the Beijing Synchrotron Radiation Facility (BSRF). All XANES spectra data were processed through background subtraction, normalization, and linear combination fitting (LCF) using Athena software.[42] The details for synchrotron analysis are presented in the Supporting Information, S1.3−S1.5.

Microbial Community Analysis. Total genomic DNA in soil samples collected at different E_h windows (soil solid phase) was extracted with a Fast DNA Spin kit (MP bio, Santa Ana, USA) using the producer's protocol. NanoDrop One (Thermo Fisher Scientific, MA, USA) was used to examine the concentration and purity of the extracted DNA (in 1% agarose gels). The DNA extractant was diluted to 1 ppb if necessary. The 16S rRNA genes of V4−V5 distinct regions were amplified using 515*F*/907R primer pairs with a 12 bp barcode.[43] The detailed syntheses of primers and polymerase chain reaction reactions, generation of sequencing libraries, and data processing are presented in the Supporting Information, S1.6.

Quality Control and Data Analysis. Triplicate/quadruplicate measurements were adopted in each analysis. Standard solutions (Merck) were employed to ensure high-quality results. The reliability of methods for total As concentration and speciation analysis was checked by comparing the dissolved As concentration measured by ICP-OES and summation of As(III) and As(V) determined by ICP-MS; values were similar (Figure S2). IBM SPSS Statistics 23 (NY, USA) was used to perform statistical analyses. OriginPro 9.1 b215 (OriginLab Corporation, Northampton, USA) was used to create figures.

RESULTS

Physical−Chemical Properties of the Soil. The studied soil had organic matter and carbonate contents of 1.20 and 3.65%, respectively, and pH 8.68 (Table S1). The carbonate was dominated by calcite, as characterized by powder X-ray diffraction (XRD) analysis. Total contents of CaO, Al_2O_3, Na_2O, K_2O, MgO, and SiO_2 were 4.80, 19.0, 0.180, 1.50, 0.500, and 51.0%, respectively. The total Fe concentration in the soil was 54,852 mg kg^{-1} (Table S1). The total S concentration in the soil was 649 mg kg^{-1}. Arsenic concentration was 3651 mg kg^{-1}, which was 36 times higher than the risk intervention value for contaminated agricultural soils defined by the Chinese government (GB15618-2018). The water-soluble As concentration was 5.50 mg kg^{-1}. The mole ratio of total Fe to total As was 20. The high total and water-soluble concentration of As in the studied soil indicates a high potential for the loss of As from the soil to groundwater and therefore high potential ecological and human health risks.

https://doi.org/10.1021/acs.est.4c02989
Environ. Sci. Technol. 2024, 58, 17850−17861

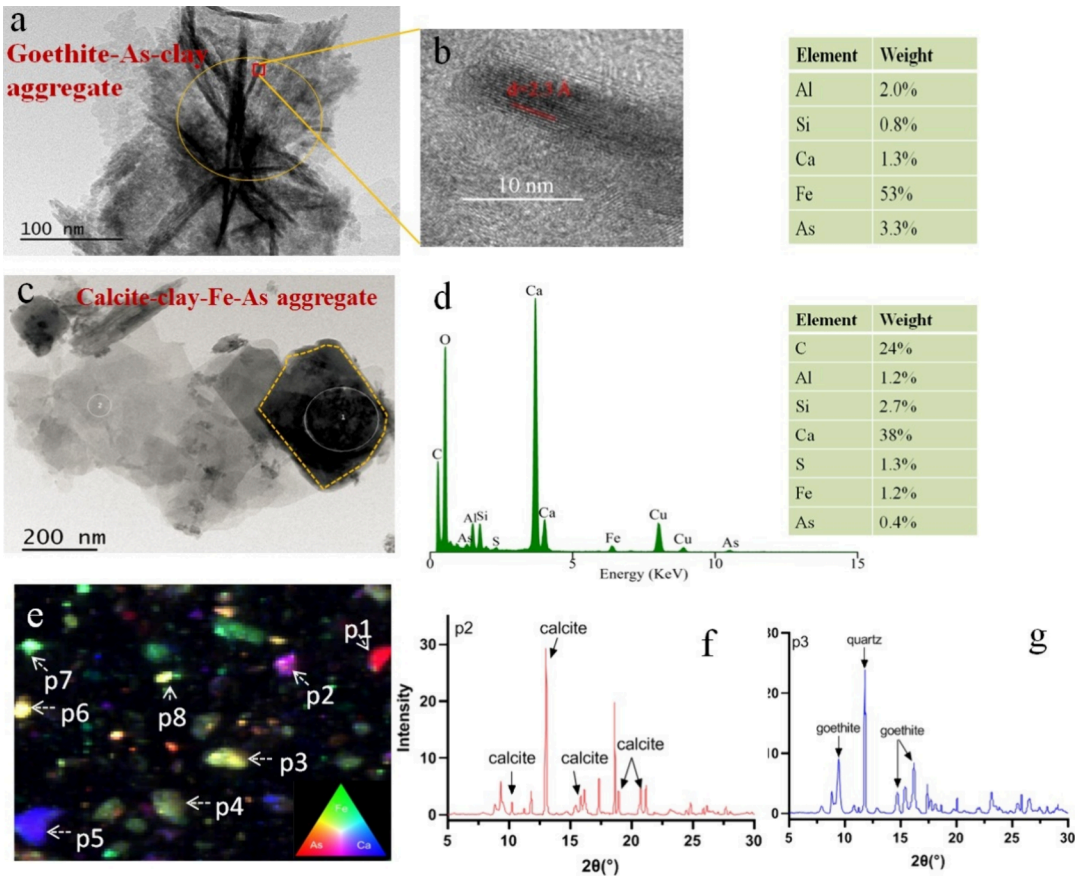

Figure 1. (a, c) Bright-field TEM image of the original soil particles. (b) HR-TEM images of goethite. (d) TEM-EDX spectrum of the analyzed particles (marked with cycles in the TEM images). Tables show the weights of elements of the particles analyzed by TEM-EDS. (e) μ-XRF images of the As, Fe, and Ca distribution in the original soil particles. (f, g) μ-XRD spectra of the spots p2 and p3.

TEM-EDS analysis was used to study the association of As with minerals in the studied soil. Results showed that As presents as calcite−clay−Fe−As, goethite−As−clay, and clay−Mn−Fe−As assembles in the soil (Figures 1a−d and S3). μ-XRF analysis further showed that the distribution of As has a rather close association with Fe in spots 3−4 and spots 6−8 (Figure 1e) and also with Ca in spots 2 and 5 (Figure 1e). The μ-XRD analysis showed the presence of goethite in spots 3−4 and 6−8 and calcite in spots 2 and 5 (Figures 1f,g and S4). μ-XANES analysis showed that As(V) is the primary As speciation in all spots 1−8 (Figure S5). Therefore, in the studied soil, goethite and calcite appear to be the important minerals that are associated with As(V) and thus could affect its release and mobilization under E_h changes.

Arsenic and Biogeochemical Factors in the Soil Liquid Phase. Flooding for 65 h lowered the slurry E_h from about 120 mV to lower than −300 mV (Figure S1). Soil slurry pH dropped rapidly after flooding and reached 6.2 at E_h of lower than −300 mV. After sampling at the E_h of about −300 mV, soil E_h was increased to 100 mV increments to achieve the highest value of about +300 mV after 420 h; further flushing with O_2 did not significantly increase the E_h greater than +300 mV. However, pH increased gradually with increasing E_h, and it was greater than 8.0 at an E_h of +200 mV (Figure S1). The decrease of pH at low E_h was in contrast to the generally reported inverse relationship between the pH and E_h. We attribute this discrepancy to the release of protons associated with decomposition of the added glucose and wheat straw.[44,45]

The dissolved As concentration increased as the E_h decreased, with high values (87−294 μM) recorded at E_h of about −300 to 0 mV, while it obviously decreased to 17−26 μM at high E_h (+100 to +300 mV) (Figures 2 and S1). The speciation of As was quantified as As(V) and As(III), with negligible organic As complexes (e.g., monomethylarsonic acid) detected (Figures 2 and S1). As(III) concentrations (76−280 μM) accounted for 87−99% of the total As at the E_h

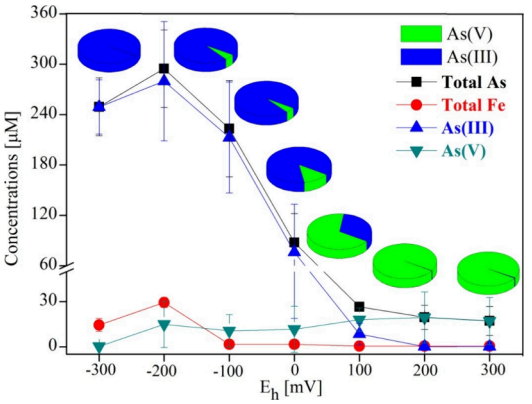

Figure 2. Dynamic of total As, As(V), As(III), and the dissolved Fe concentrations in the soil liquid phase as a function of E_h changes. Error bars represent the standard deviation from three replicates. Pie charts above each error bar indicate the proportion of As(V) and As(III) in the soil liquid phase.

https://doi.org/10.1021/acs.est.4c02989
Environ. Sci. Technol. 2024, 58, 17850−17861

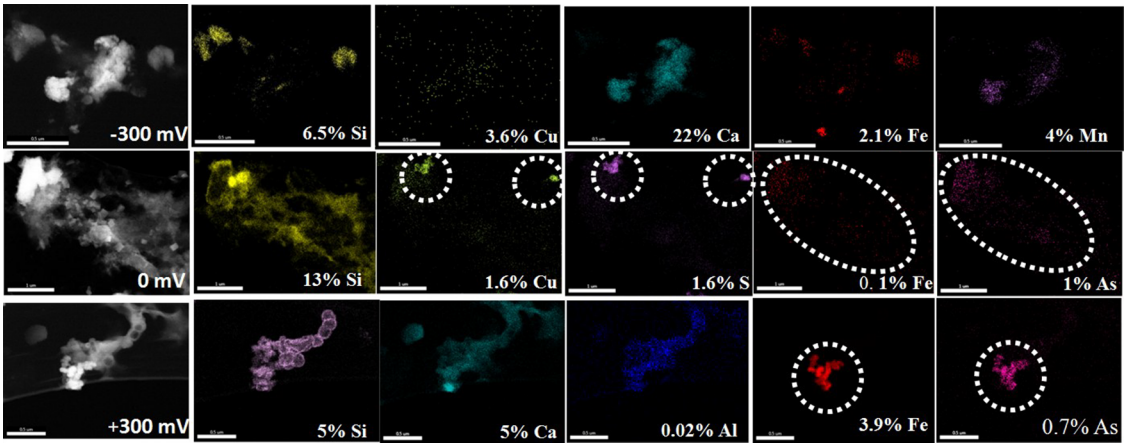

Figure 3. Environmental scanning electron microscope (ESEM) images of the colloids collected at the predefined E_h of −300 mV, 0 mV, and +300 mV, and ESEM-energy-dispersive spectroscopy (EDS) digital images of silicon (Si), calcium (Ca), copper (Cu), manganese (Mn), iron (Fe), arsenic (As), aluminum (Al), and sulfur (S). The white dashed circles indicate a similar distribution pattern of Fe and As at the predefined E_h values of 0 and +300 mV. The ESEM images of other elements are shown in Figure S6. % means the mass weight ratio of the element of the analyzed sample. Note: We did not detect As in the colloid at the predefined E_h of −300 mV, and Mn at both 0 and +300 mV.

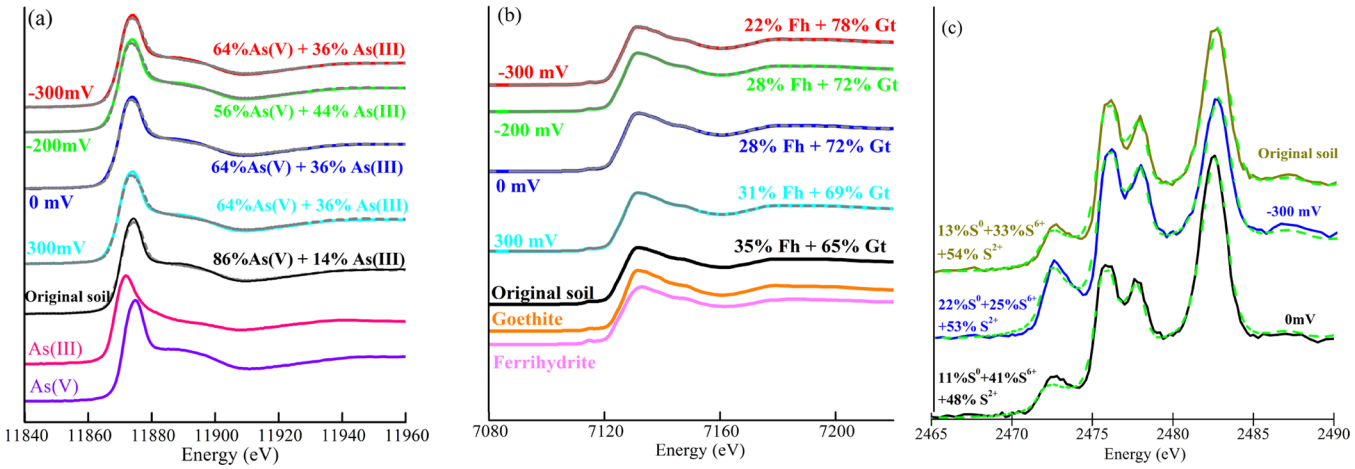

Figure 4. (a) Arsenic K-edge XANES spectra and (b) iron K-edge XANES spectra of the original soil and the soil solid phase collected at predefined E_h of −300, −200, 0, and 300 mV. (c) Sulfur K-edge XANES spectra of the original soil and the soil solid phase collected at predefined E_h of −300 and 0 mV. The different proportions of As, Fe, and S obtained from the LCF at different E_h windows were labeled adjacent to each spectrum. Go means goethite, and Fh means ferrihydrite. Solid lines represent the spectra of soils and standards, while gray or green dashed lines represent the LCF curves.

zone of −300 to 0 mV (Figures 2 and S1). The raising of E_h over +100 mV decreased As(III) to 0.07−8.5 μM but increased As(V) (Figures 2 and S1, 17−19 μM, 68−99% of the total As).

The dissolved Fe concentration (14−29 μM) at the E_h zone of −300 to −200 mV was 41−82 times higher than that at E_h −100 to +300 mV (0.36−1.6 μM) (Figures 2 and S1). It decreased rapidly for E_h greater than −100 mV (Figures 2 and S1). The dissolved Ca concentrations at the E_h zone of −300 to −100 mV were 9.0−14.8 mM, and they began to decrease at an E_h of 0 mV and reached the lowest value at an E_h value of +200 mV (Table S2). Sulfate concentrations decreased as a function of E_h, with the highest value at an E_h of −200 mV (0.73 mM) and the lowest value presented at an E_h of +200 mV (0.33 mM) (Table S2). The concentration of dissolved Cu showed a different response to changing E_h compared with that of Fe and Ca (Table S2). It was at a maximum across the E_h range of +100 to +300 mV (0.47−0.57 μM), followed by −300 to −200 mV (0.07−0.09 μM), and was the lowest for the range of −100 to 0 mV (<0.01 μM). DOC concentration is E_h-dependent, and it decreased with increasing E_h (Table S2).

Arsenic in the Colloidal Phase. We performed SEM-EDX analysis of the colloids collected at E_h values of −300, 0, and +300 mV (Figures 3 and S6). There was a similar distribution pattern between Ca and O in the colloids collected at different E_h windows (Figures 3 and S6), indicating the presence of calcium carbonate. Also, there was a similar distribution pattern between Fe and As at E_h values of 0 mV and 300 mV and between Cu and S at an E_h value of 0 mV (Figure 3, marked with the white dashed circles), suggesting the adsorption of As onto Fe oxides and the formation of CuS in the colloids. The similar distribution among Ca, Si, and Al might indicate the presence of calcium aluminum silicate.

Redox Chemistry of Arsenic, Iron, and Sulfur in the Soil Solid Phase. Arsenic speciation in the original soil and the soil solid phase collected at E_h values of −300, −200, 0, and +300 mV was analyzed with As K-edge XANES spectroscopy (Figure 4a). Principal component analysis and

https://doi.org/10.1021/acs.est.4c02989
Environ. Sci. Technol. 2024, 58, 17850−17861

LCF indicated that XANES spectra of As could be reconstructed using XANES spectra data for Fe(oxyhydr)-oxide-bound As(V) and As(III) (Table S3). Arsenic in the original soil was characterized as 86% As(V) and 14% As(III). Flooding of soil (−300 mV) led to a reduction in the proportion of As(V) to 64% and an increase in the As(III) proportion to 36% (Figure 4a). A gradual increase of E_h to −200 mV decreased the proportion of As(V) to 56% and increased As(III) to 44% (Figure 4a). It appears that the low E_h windows are favorable for the conversion of As(V) to As(III). Further increase in E_h to 0 mV increased the proportion of As(V) to 64%; however, there was no more change in relative speciation as the E_h increased to +300 mV.

Iron speciation in the original soil and soil solid phase collected at E_h values of −300, −200, 0, and +300 mV were analyzed with Fe K-edge XANES spectroscopy (Figure 4b and Table S4). Relative Fe speciation in the original soil was 65% goethite and 35% ferrihydrite. The dominance of goethite was consistent with our μ-XRD result. The relative proportion of ferrihydrite decreased to 22−28% at E_h of −300 to 0 mV. This decrease in ferrihydrite was associated with an increase in the abundance of goethite (72−78% at E_h of −300 to 0 mV), accounting for nearly all of the change in ferrihydrite. This phenomenon is likely due to the recrystallization of ferrihydrite to goethite. The relative abundance of ferrihydrite increased slightly at an E_h over 0 mV and then remained relatively consistent between 0 and +300 mV.

Sulfur speciation in the original soil and in the soil solid phase collected at the predefined E_h of −300 and 0 mV was analyzed with S K-edge XANES spectroscopy (Figure 4c and Table S5). The relative speciation of S in the original soil was 54% S^{2+}, 33% S^{6+}, and 13% zerovalent sulfur (S^0). Changes in S speciation were redox-dependent. Flooding of soil to an E_h of −300 mV decreased the proportion of S^{6+} to 25% and increased S^0 to 22%. The subsequent increase of E_h to 0 mV decreased the proportion of S^0 to 11% and increased S^{6+} to 41%. The proportion of S^{2+} remained relatively stable (48%−53%) throughout the studied E_h zones (−300 to 0 mV).

Key Microbial Community Composition in the Soil Solid Phase. Among the identified bacteria, *Bacillus* spp., *Clostridium* spp., *Desulfitobacterium* spp., *Pseudomonas* spp., and *Stenotrophomonas* spp. are likely to be involved in the transformation of As in our soil (Figure S7). The relative abundance of *Clostridium* spp, *Desulfitobacterium* spp, and *Bacillus* spp. was greater in the anaerobic environment and reduced with increasing E_h (Figure S7). In contrast, *Pseudomonas* spp. and *Stenotrophomonas* spp. had a greater relative abundance at high E_h windows. Both *Desulfitobacterium* spp. and *Pseudomonas* spp. showed lower relative abundance than *Bacillus* spp., *Clostridium* spp., *Achromobater* spp., and *Stenotrophomonas* spp.

DISCUSSION

Mechanism of Arsenic Desorption and Reduction in the Soil. A minor amount of As(III) as determined by bulk XANES in the original soil was likely due to the formation of bidentate binuclear surface complexes on iron oxides (e.g., goethite), which protected As(III) from oxidation.[46,47] It was reported that the complexation of As(III) on the surface of goethite could yield an average As(III)−Fe interatomic distance of 3.378 ± 0.014 Å, which is indicative of bidentate binuclear bridging As(III) complexes on the α-FeOOH surface.[47] However, the μ-XANES analyses did not detect As(III) presumably due to the spatial heterogeneity of the studied soil. In addition to Fe(oxyhydr)oxides (Figure 1e−g), a close association of As(V) and calcite was observed, which was in line with a previous report that calcite preferentially immobilized As(V) through sorption or coprecipitation processes.[48] The original soil exhibited an Fe/As mole ratio of 20, surpassing the previously recorded range in sediments (0.3−1.1),[49,50] where Fe oxides have been shown to efficiently scavenge dissolved As from the liquid phase. The Fe/As ratio in our soil is therefore expected to characterize the ability of the soil to scavenge As. Nevertheless, the water-soluble As concentration was unexpectedly high at 5.5 mg kg^{-1}, likely due to the alkaline pH, which impairs the chemisorption of As(V) and diminishes the binding affinity of Fe oxides.[51]

The recorded dissolved As concentrations during redox changes in the MCs (87−294 μM) were 9−32 times higher than the water-soluble As concentration (9.2 μM) in the original soil (Figure 2). This substantial difference provides compelling evidence that As-bearing minerals play a significant role in As mobilization (reductive, proton, and ligand). A significant positive correlation between the dissolved Fe and dissolved As concentrations suggested the promotion of As mobilization via the dissimilatory reduction of As-bearing Fe minerals (Figure 5a). Both ferrihydrite and goethite are present

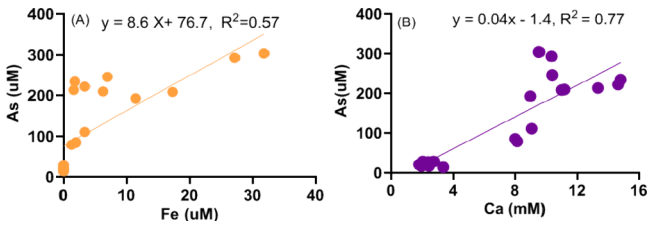

Figure 5. (A) Relation between the dissolved Fe and As, and (B) the dissolved Ca and As in the soil liquid phase across the E_h zones. n = 21.

in our soil, and the fractional amount of ferrihydrite decreased significantly at an E_h of −300 mV compared to the original soil (Figure 4b). This is because the high surface area and great reactivity of ferrihydrite (ΔG_{rxn} = −43 kJ mol^{-1}) made it more thermodynamically favorable for dissimilatory reduction than goethite (ΔG_{rxn} = −6.4 kJ mol^{-1}).[52] Additionally, the reductive dissolution of ferrihydrite can also occur via a sulfide-catalyzed reaction under sulfidogenic conditions (eq 1).[53] We expected the occurrence of this reaction in the soil at low E_h windows, as supported by the presence of the significant amount of S^0 at an E_h value of −300 mV compared to the original soil (increased by 9%) (Figure 4c and Table S5).

$$2Fe(OH)_3 + HS^- + 5H^+ \rightarrow 2Fe^{2+} + S^0 + 6H_2O \quad (1)$$

In addition to the reductive dissolution of Fe oxides, the dissolution of calcite also contributes to As mobilization. As shown in Figure 1e−f, some As were associated with calcite in the soil. The low pH at an E_h value of −300 mV of the soil shall facilitate the dissolution of calcite, leading to the release of Ca and As associated with calcite. This is supported by the positive correlation between dissolved Ca and dissolved As in the soil liquid phase (Figure 5b, R^2 = 0.77, p < 0.001).

Arsenic was primarily present as As(III) in the soil liquid phase at low E_h windows (−300 to 0 mV) (Figure 2). This could be due to the desorption of As(III) from the soil As(III) pool and the reduction of soil As(V). Since the original soil

https://doi.org/10.1021/acs.est.4c02989
Environ. Sci. Technol. 2024, 58, 17850−17861

contains As(III), it is possible that the desorption of labile, outer-sphere As(III) complexes and complexes located on exterior surface sites might be contributing to As(III) in the soil liquid phase. Assuming that As(III) desorption was predominant in the soil, the proportion of As(III) should have decreased. In reality, the proportion of As(III) in the soil at an E_h of −300 mV increased by 22% compared to the original soil (Figure 4a and Table S3). Therefore, the contribution of As(III) desorption from the soil As(III) pool is relatively minor. Alternatively, the reduction of soil As(V) is expected to be the dominant process affecting aqueous As(III) in the soil. Certain bacteria belonging to the genera *Bacillus*, *Clostridium*, *Desulfitobacterium*, and *Pseudomonas* possess arsenate reductase, an enzyme capable of catalyzing the reduction of As(V).[54] This reduction occurs subsequent to the diffusion or uptake of As(V) into the cytoplasmic space. Consequently, the reduction of As(V) takes place after its liberation from Fe(oxyhydr)oxides. Notably, this desorption and reduction process is remarkably swift, as evidenced by the negligible levels of As(V) detected in the liquid phase of the soil after just 48 h of incubation (Figure 2).

Sequestration of Arsenic by Fe(oxyhydr)oxides. The variation of E_h resulted in the change of the relative proportion of ferrihydrite and goethite in the soil solid phase (Figure 4b and Table S4). We attributed this phenomenon to the recrystallization of ferrihydrite to goethite catalyzed by Fe(II). The Fe^{2+}-catalyzed transformation of ferrihydrite to goethite is rapid under room temperature, achieving a conversion rate constant of 4.0×10^{-5} 1/s at 21 °C.[55] Further, the increase in reaction temperature can increase the constant by orders of magnitude. Hansel et al.[56] found that the presence of 40 μM Fe^{2+} resulted in a 90% conversion of 2-line ferrihydrite to goethite and lepidocrocite within 120 min under advective flow conditions. Further, the recrystallization of Fe oxides can be enhanced by carbonate,[57] which presented in our soil. Fe(II) was utilized during the recrystallization of the Fe phase, and thus its availability was reduced.[58] Generally, the concomitant release of both Fe and As via the dissimilatory reduction of As-bearing Fe(oxyhydr)oxides typically results in a high Fe/As mole ratio in solution, consistent with the Fe/As ratio of the solid (or surface layers). For example, Fe/As mole ratios ranging from 154 to 669 were observed in solutions from As-contaminated soil (with a total Fe content of 32.1 g kg^{-1} and a total As content of 164 mg kg^{-1}) collected from Zhejiang province in China.[59] Our soil solid phase had an Fe/As mole ratio of 20, but that in the liquid phase was only 0.01−0.1 (Figure S8), proving a significant elimination of aqueous Fe(II).

Further, the microaerophilic conditions promote Fe precipitation.[60] As the E_h of the soil exceeded −200 mV, the pH shifted toward alkalinity, resulting in the oxidation of Fe(II) and its subsequent precipitation as Fe(oxyhydr)oxides, thus eliminating its availability. The XANES results showed a slight increase of ferrihydrite by 6% in the soil solid phase at an E_h of 0 mV relative to −300 mV (Figure 4b). The newly formed Fe(oxyhydr)oxides (likely as ferrihydrite) can sorb As, as further confirmed by the coprecipitation of Fe and As in the colloids at $E_h \geq 0$ mV (Figure 3).

The variation of As speciation in the soil solid phase as a function of E_h corroborated the liquid phase data (Figures 4a and 2). The proportion of soil As(III) (bound with Fe(oxyhydr)oxides) increased by 22% at an E_h of −300 mV (Figure 4a and Table S3), corresponding to the highest concentration of As(III) in the soil liquid phase (280 μM) (Figure 2). It appears that most of the mobilized As(III) was retained by Fe(oxyhydr)oxides, while the remaining As(III) entered the soil liquid phase. Binding of As(III) by Fe(oxyhydr)oxides was noticeable under neutral to alkaline conditions.[51] Further, it has been reported that the recrystallization of Fe(oxyhydr)oxides (e.g., from ferrihydrite to goethite) can lead to the incorporation of As(III) into secondary Fe oxide minerals.[61] The extent to which As(III) is retained in these secondary Fe oxides will depend on their specific properties. For example, the newly formed siderite or green rust is less efficient in binding As than goethite or magnetite.[61,62] Here, the newly formed goethite, resulting from the recrystallization of ferrihydrite upon the onset of reducing conditions (−300 to −200 mV), might sorb As(III). This finding further confirms the previous result, obtained based on the desorption of As from ferrihydrite-coated sands presorbed with As(III), that the retention of As(III) only depends on the recrystallization of ferrihydrite to goethite or magnetite.[63] Additionally, the labile carbon plays a critical role in the adsorption of As(III) by the secondary ferrous/ferric phases. The limited amount of labile carbon can restrain the microbially mediated Fe(oxyhydr)oxide reduction, leading to the poor retention of As(III) through the newly formed Fe oxides. Here, glucose and wheat straw were added to the microcosms to prevent any carbon-limitation effect on microbial growth. The stimulation of microorganisms could have increased the Fe(oxyhydr)oxide reduction rate, promoting the retention of As(III) by the newly formed ferric phases (e.g., goethite).[64] The retention of As(III) by the "old" ferric phases (e.g., original goethite) in our soil is expected to be of minor importance. This is due to their association with aggregates of organic matter, $CaCO_3$, and clay minerals (Figure 1a−c), which, in turn, decreases the surface area of Fe(oxyhydr)oxides, ultimately restricting the adsorption of As(III).

The proportion of As(III) bound to Fe(oxyhydr)oxides remained relatively constant across a range of E_h values from −200 to +300 mV (Figure 4a and Table S3), suggesting the persistent presence of As(III) in the soil. It appears that As(III) bound to the newly formed ferric phase was resistant to oxidation. We proposed that the newly formed ferric phase might adsorb/incorporate As(III), thereby shielding it from oxidation. Zhang et al.[65] found that about 50−90% of the added As(III) and As(V) became more stable during the Fe(II)-catalyzed recrystallization of As-adsorbed ferrihydrite. They attributed this phenomenon to the incorporation of As into the structure of the crystallized products.

Microorganisms Responsible for Arsenic Transformations. *Bacillus* spp., *Clostridium* spp., *Desufitobacterium* spp., and *Pseudomonas* spp. are important in the transformation of As in the soil (Figure S7). Bacteria belonging to *Bacillus* spp. (e.g., *B.selenitireducens* strain MLS10),[66−69] *Clostridium* spp.[70] (e.g., *Clostridium* spp. CN, *Sulfurospirillum arsenophilum*),[71,72] *Desufitobacterium* spp.,[73−76] *Pseudomonas* spp. (e.g., APSLA3 and MP1400),[77,78] and *Geobacter* spp. possess the ability to reduce both As(V) and Fe(III). These bacteria, capable of reducing As(V), express the arsenate reductase gene,[79] which is located in the outer membrane and periplasm of bacteria.[80,81] Some bacteria belonging to *Stenotrophomonas* have been documented as an As(III) oxidizer.[82] *Stenotrophomonas* exhibited a high relative abundance at high E_h windows (+100 to +300 mV). Thus, it is likely to play a role in As(III)

https://doi.org/10.1021/acs.est.4c02989
Environ. Sci. Technol. 2024, 58, 17850−17861

oxidation in our soil under high E_h. It should be noted that the potential As(V) reducers such as *Pseudomonas* spp. exhibited a considerable relative abundance within high E_h windows, but they unlikely promoted the As(III) level because of its oxidation to As(V) via both microbial (e.g., *Stenotrophomonas*) and abiotic processes.

Effect of DOC and Sulfate on Arsenic Mobilization and Sequestration. The highest DOC concentration presented at low E_h windows was attributed to the decomposition of straw as well as the interaction of glucose itself. The continuous decrease of DOC as a function of E_h was likely due to both microbial consumption and the adsorption onto Fe(oxyhydr)oxides.[39,83] The presence of higher dissolved As and DOC at low E_h zones is consistent with the hypothesis that organic carbon promotes the microbially mediated reductive dissolution of As. Further, a significant positive correlation between DOC and dissolved As/dissolved Fe (Figure S9) suggests that DOC may promote As desorption by inducing Fe oxide dissolution.[84] Further, the aromatic and terrestrially derived fulvic acid of DOC can enhance As mobilization by promoting As−Fe−DOC complexation reactions.[85]

The higher sulfate concentration in the liquid phase presented lower E_h values (Table S2). We attributed this phenomenon to the fact that the reductive dissolution of Fe(oxyhydr)oxides (e.g., ferrihydrite) liberated the associated sulfate. The slight decrease of the fractional amount of sulfate (S^{6+}) in the soil at an E_h of −300 mV compared to the original soil further supported the liberation of sulfate from soil Fe(oxyhydr)oxides (Figure 4c). At a high SO_4^{2-} concentration (∼70 mg L^{-1}) and pH value greater than 5.0, the dissimilatory reduction of SO_4^{2-} can competitively inhibit the reduction of As(V) and Fe^{3+}.[83,86] This is particularly the case when the Gibbs free energy change (ΔG^0) for dissimilatory sulfate or Fe oxide reduction is equally favorable.[87] Preferential or concurrent SO_4^{2-} reduction may preserve the sorbed As(V) and prevent its release.[83] Given that the sulfate concentration was approximately 0.63−0.73 mM in the soil liquid phase at the E_h zone of −300 ∼ −200 mV and pH > 6.5 (Figure S1 and Table S2), it is likely that the dissimilatory reduction of SO_4^{2-} had an impact on Fe oxide reduction, which subsequently influenced As release. Sulfide can bind with As(III)/As(V) to form As_2S_3 and arsenian pyrite.[88,89] In the soil solid phase, we failed to detect As_2S_3 and arsenian pyrite using XANES spectroscopy (Figure 4a), which indicates a minor effect of sulfide on As. This is likely due to the consumption of sulfide within various biogeochemical reactions during redox changes.[90] As mentioned earlier, the sulfide-catalyzed reductive dissolution of ferrihydrite utilizes sulfide for the production of S^0 and Fe^{2+}. The occurrence of this reaction in our soil was confirmed by the presence of S^0 (Figure 4c). Further, the presence of CuS in the colloid at an E_h of 0 mV suggested the scavenging of sulfide through binding to Cu^{2+} (Figures 3 and S6).

Environmental Implication. Soils and sediments contain abundant Fe(oxyhydr)oxides, which primarily control the geochemical behavior of As. The abundance and types of Fe(oxyhydr)oxides and the reductive dissolution ability of Fe(oxyhydr)oxides strongly affect the desorption of As, etc.[91,92] In a typical karstic soil highly contaminated with As, besides Fe(oxyhydr)oxides, it possesses abundant carbonate minerals (e.g., calcite), which can serve as an As reservoir via incorporation of both As(V) and As(III) into calcite crystals or be incorporated during calcite growth.[93] Both the reductive dissolution of Fe(oxyhydr)oxides and acidic dissolution of calcite led to the release of As(V) followed by its reduction to As(III) under anaerobic conditions. Most of the mobilized As(III) was sequestered by the recrystallized Fe(oxyhydr)-oxides (e.g., goethite). The recrystallization of ferrihydrite into more stable Fe(III) oxides (e.g., goethite) appears to be an important sequestration mechanism for As(III) in karstic soil. It should be noted that although most As(III) was sequestered by the ferric phases, As(V) reduction still triggered a significant release of As(III) into the soil liquid phase upon flooding. The dissolved As(III) concentration (14.4−22.7 mg L^{-1}) under low E_h windows (−300 to −100 mV) was almost 3 orders of magnitude higher than the maximum allowable As concentration in the drinking water (0.01 mg L^{-1}) as defined by the World Health Organization and approximately 3-fold over the toxicity characteristic leaching procedure limit (5 mg L^{-1}).

Our findings are fundamental for assessing the environmental risks associated with As contamination in soils across global karst regions, encompassing southwestern China, southeastern Asia, the Mediterranean, and North America. An environmental hazard stemming from As in flooded or anaerobic soils, specifically in karst regions with exogenous carbon inputs, is particularly pronounced when As has the potential to readily infiltrate groundwater via pipes, cracks, vents, and sinkholes.[94] In the context of climate change, our research highlights flooding and the leaching of soil carbon from straw decomposition and dead plant matter as the primary drivers of As mobilization in karstic soils.

Also, our findings provide valuable insights into practical strategies for managing As risks. We advise against transitioning from dry cropping or pasture to paddy rice production in karst regions as this can potentially reduce the redox potential. Also, the change of cropping system from water-lodged rice to ridge-cultivated rice can increase the redox potential of soil, leading to the decrease of As mobility.[95] Moreover, the amendment of oxygen-based amendments such as hydrogen peroxide can also be an option to increase the redox potential of soil.[96] By enhancing the E_h value, over 90% of soluble As in the soil solution can be removed through mechanisms such as coprecipitation/adsorption with Fe-(oxyhydr)oxides. This presents a promising strategy for mitigating the risk of As leaching into groundwater through the application of Fe-based amendments. Future research is crucial to monitor the behavior of As and its governing factors in karstic soils under natural conditions as well as to assess the effectiveness of Fe-based amendments in minimizing the risk of As contamination in groundwater.

■ ASSOCIATED CONTENT

Supporting Information

The Supporting Information is available free of charge at https://pubs.acs.org/doi/10.1021/acs.est.4c02989.

Additional experimental details; synchrotron data analysis; microbial community analysis; pH−E_h plot of the soil for each microcosm; dissolved arsenic concentration measured by both ICP-OES and ICP-MS; TEM image and TEM-EDX spectrum of soil particles; μ-XRD spectra of soil particles; normalized μ-XANES spectra of soil particles; ESEM images of the colloidal phase and EDS image of elements; relative abundance of key microorganisms; Fe/As ratios in the

https://doi.org/10.1021/acs.est.4c02989
Environ. Sci. Technol. 2024, 58, 17850−17861

soil liquid phase; relation between dissolved Fe/As and DOC; physical and chemical properties of the original soil; concentrations of Ca, sulfate, dissolved Cu, and DOC in the soil liquid phase; and LCF of XANES spectra (PDF)

AUTHOR INFORMATION

Corresponding Authors

Jianxu Wang − *State Key Laboratory of Environmental Geochemistry, Institute of Geochemistry, Chinese Academy of Sciences, 550082 Guiyang, P.R. China; University of Wuppertal, School of Architecture and Civil Engineering, Institute of Foundation Engineering, Water- and Waste-Management, Laboratory of Soil- and Groundwater-Management, 42285 Wuppertal, Germany;* orcid.org/0000-0001-9198-0144; Email: wangjianxu@vip.gyig.ac.cn

Jörg Rinklebe − *University of Wuppertal, School of Architecture and Civil Engineering, Institute of Foundation Engineering, Water- and Waste-Management, Laboratory of Soil- and Groundwater-Management, 42285 Wuppertal, Germany;* orcid.org/0000-0001-7404-1639; Email: rinklebe@uni-wuppertal.de

Authors

Sabry M. Shaheen − *University of Wuppertal, School of Architecture and Civil Engineering, Institute of Foundation Engineering, Water- and Waste-Management, Laboratory of Soil- and Groundwater-Management, 42285 Wuppertal, Germany*

Ann-Christin Swertz − *Faculty of Mechanical Engineering and Safety Engineering, Department of Safety Technology and Environmental Protection, University of Wuppertal, 42119 Wuppertal, Germany*

Chengshuai Liu − *State Key Laboratory of Environmental Geochemistry, Institute of Geochemistry, Chinese Academy of Sciences, 550082 Guiyang, P.R. China;* orcid.org/0000-0003-0133-0119

Christopher W.N. Anderson − *Environmental Sciences, School of Agriculture and Environment, Massey University, 4442 Palmerston North, New Zealand;* orcid.org/0000-0003-0935-1475

Scott Fendorf − *Department of Earth System Science, Stanford University, Stanford, California 94305, United States;* orcid.org/0000-0002-9177-1809

Shan-Li Wang − *Department of Agricultural Chemistry, National Taiwan University, Taipei 106, Taiwan ROC;* orcid.org/0000-0003-3156-5365

Xinbin Feng − *State Key Laboratory of Environmental Geochemistry, Institute of Geochemistry, Chinese Academy of Sciences, 550082 Guiyang, P.R. China; University of Chinese Academy of Sciences, Beijing 100049, PR China*

Complete contact information is available at: https://pubs.acs.org/10.1021/acs.est.4c02989

Notes

The authors declare no competing financial interest.

ACKNOWLEDGMENTS

The authors thank the National Natural Science Foundation of China (42222305), the German Alexander von Humboldt Foundation (ref 3.5-1186537-CHN-HFST-P), the Guizhou Provincial 2020 Science and Technology Subsidies (No. GZ2020SIG), the Fundamental Research Program of the Department of Science and Technology of Guizhou (ZK[2021]-key-045), the Pioneer Hundred-Talent Program of Chinese Academy of Sciences, the Guizhou thousand talents innovation and entrepreneurship plan (GZQ202208090), and the Opening Fund of the State Key Laboratory of Environmental Geochemistry (SKLEG2024209) for financial support. This research used the 4-BM beamline of the National Synchrotron Light Source II, a U.S. Department of Energy (DOE) Office of Science User Facility operated for the DOE Office of Science by Brookhaven National Laboratory under Contract No. DE-SC0012704. The authors sincerely thank the staff at beamline 07 A and beamline 17C at NSRRC and the staff at beamline 4B7A at BSRF for assistance during acquisition of the XAS spectra. The authors also thank Dr. J. G. Xu for assistance during the processing of μ-XRD data.

REFERENCES

(1) Ford, D. C.; Williams, P. W. *Karst geomorphology and hydrology*; Unwin Hyman London, 1989; Vol. *601*.

(2) Hu, R.; Fu, S.; Xiao, J. Major scientific problems on low-temperature metallogenesis in South China. *Acta Petrol. Sin.* **2016**, *32* (11), 3239−3251.

(3) Wang, J.; Xing, Y.; Li, P.; Xia, J.; Liu, T.; Feng, X. Chemically-assisted phytoextraction from metal(loid)s-polluted soil at a typical carlin-type gold mining area in southwest China. *J. Cleaner Prod.* **2018**, *189*, 612−619.

(4) Wang, S.-J.; Li, R.-L.; Sun, C.-X.; Zhang, D.-F.; Li, F.-Q.; Zhou, D.-Q.; Xiong, K.; Zhou, Z.-F. How Types of Carbonate Rock Assemblages Constrain the Disribution of Karst Rocky Desertified Land in Guizhou Province, PR China: Phenomena and Mechanisms. *Land Degrad. Dev.* **2004**, *15*, 123−131.

(5) Silva, M. B.; dos Anjos, L. H. C.; Pereira, M. G.; Schiavo, J. A.; Cooper, M.; de Cavassani, R. S. Soils in the Karst Landscape of Bodoquena Plateau in Cerrado Region of Brazil. *CATENA* **2017**, *154*, 107−117.

(6) Mendez, J. C.; Hiemstra, T. Carbonate Adsorption to Ferrihydrite: Competitive Interaction with Phosphate for Use in Soil Systems. *ACS Earth Space Chem.* **2019**, *3* (1), 129−141.

(7) Sun, Y.; Niazi, N. K.; Wang, J. Arsenic Contamination in Karst Regions. In *Global Arsenic Hazard*; Niazi, N. K., Bibi, I., Aftab, T., Ed.; Springer Cham Press, 2023; pp 85−98.

(8) Jiang, J.; Wang, X.; Su, C.; Wang, M.; Ren, F.; Huq, Md. E. Unraveling the Impact of Dissolved Organic Matter on Arsenic Mobilization in Alluvial Aquifer of the Lower Yellow River Basin, Northern China. *Appl. Geochem.* **2023**, *158*, No. 105781.

(9) Yi, H.; Cui, J.; Sun, J.; Zhou, X.; Ye, T.; Gan, S.; Chen, J.; Yang, Y.; Liang, W.; Guo, P.; Abdelhaleem, A.; Xiao, T. Key Drivers Regulating Arsenic Enrichment in Shallow Groundwater of the Pearl River Delta: Comprehensive Analyses of Iron, Competitive Anions, and Dissolved Organic Matter. *Appl. Geochem.* **2023**, *151*, No. 105602.

(10) Tufano, K. J.; Reyes, C.; Saltikov, C. W.; Fendorf, S. Reductive Processes Controlling Arsenic Retention: Revealing the Relative Importance of Iron and Arsenic Reduction. *Environ. Sci. Technol.* **2008**, *42* (22), 8283−8289.

(11) Wang, J.; Zeng, X.-C.; Zhu, X.; Chen, X.; Zeng, X.; Mu, Y.; Yang, Y.; Wang, Y. Sulfate Enhances the Dissimilatory Arsenate-Respiring Prokaryotes-Mediated Mobilization, Reduction and Release of Insoluble Arsenic and Iron from the Arsenic-Rich Sediments into Groundwater. *J. Hazard. Mater.* **2017**, *339*, 409−417.

(12) Saltikov, C. W.; Newman, D. K. Genetic Identification of a Respiratory Arsenate Reductase. *Proc. Natl. Acad. Sci. U. S. A.* **2003**, *100* (19), 10983−10988.

(13) Lopez-Adams, R.; Newsome, L.; Moore, K. L.; Lyon, I. C.; Lloyd, J. R. Dissimilatory Fe(III) Reduction Controls on Arsenic

Mobilization: A Combined Biogeochemical and NanoSIMS Imaging Approach. *Front. Microbiol.* **2021**, *12*, No. 640734.
(14) Gorny, J.; Billon, G.; Lesven, L.; Dumoulin, D.; Madé, B.; Noiriel, C. Arsenic Behavior in River Sediments under Redox Gradient: A Review. *Sci. Total Environ.* **2015**, *505*, 423−434.
(15) Liu, X.; Cai, X.; Wang, P.; Yin, N.; Fan, C.; Chang, X.; Huang, X.; Du, X.; Wang, S.; Cui, Y. Effect of Manganese Oxides on Arsenic Speciation and Mobilization in Different Arsenic-Adsorbed Iron-Minerals under Microbially-Reducing Conditions. *J. Hazard. Mater.* **2023**, *445*, No. 130602.
(16) Arai, Y.; Sparks, D. Residence Time Effects on Arsenate Surface Speciation At the Aluminum Oxide-Water Interface. *Soil Sci.* **2002**, *167*, 303−314.
(17) Chen, M.; Xie, Z.; Yang, Y.; Gao, B.; Wang, J. Contrasting Effects of Dissimilatory Fe(III)/As(V) Reduction on Arsenic Mobilization of Al Coprecipitated Ferrihydrite in Simulated Groundwater. *Chem. Geol.* **2023**, *639*, No. 121731.
(18) Solaiman, A. R. M.; Meharg, A. A.; Gault, A. G.; Charnock, J. M. Arsenic Mobilization from Iron Oxyhydroxides Is Regulated by Organic Matter Carbon to Nitrogen (C:N) Ratio. *Environ. Int.* **2009**, *35* (3), 480−484.
(19) Wolthers, M.; Butler, I. B.; Rickard, D. Influence of Arsenic on Iron Sulfide Transformations. *Chem. Geol.* **2007**, *236* (3), 217−227.
(20) Kim, M.-J.; Nriagu, J.; Haack, S. Carbonate Ions and Arsenic Dissolution by Groundwater. *Environ. Sci. Technol.* **2000**, *34* (15), 3094−3100.
(21) Appelo, C. A. J.; Van Der Weiden, M. J. J.; Tournassat, C.; Charlet, L. Surface Complexation of Ferrous Iron and Carbonate on Ferrihydrite and the Mobilization of Arsenic. *Environ. Sci. Technol.* **2002**, *36* (14), 3096−3103.
(22) Bia, G.; García, M. G.; Rueda, E. S.; Mors, R. A.; Mlewski, E. C.; Gomez, F. J.; Borgnino, L. Arsenic in Natural Carbonates: The Role of the Biogeochemical Conditions in Its Solid Speciation. *Chem. Geol.* **2021**, *583*, No. 120477.
(23) Sø, H. U.; Postma, D.; Jakobsen, R.; Larsen, F. Sorption and Desorption of Arsenate and Arsenite on Calcite. *Geochim. Cosmochim. Acta* **2008**, *72* (24), 5871−5884.
(24) Shimizu, M.; Zhou, J.; Schröder, C.; Obst, M.; Kappler, A.; Borch, T. Dissimilatory Reduction and Transformation of Ferrihydrite-Humic Acid Coprecipitates. *Environ. Sci. Technol.* **2013**, *47* (23), 13375−13384.
(25) Chen, G.; Hofstetter, T. B.; Gorski, C. A. Role of Carbonate in Thermodynamic Relationships Describing Pollutant Reduction Kinetics by Iron Oxide-Bound Fe2+. *Environ. Sci. Technol.* **2020**, *54* (16), 10109−10117.
(26) Vikesland, P. J.; Valentine, R. L. Iron Oxide Surface-Catalyzed Oxidation of Ferrous Iron by Monochloramine: Implications of Oxide Type and Carbonate on Reactivity. *Environ. Sci. Technol.* **2002**, *36* (3), 512−519.
(27) Pigna, M.; Caporale, A. G.; Cavalca, L.; Sommella, A.; Violante, A. Arsenic in the Soil Environment: Mobility and Phytoavailability. *Environ. Eng. Sci.* **2015**, *32* (7), 551−563.
(28) Darland, J. E.; Inskeep, W. P. Effects of pH and Phosphate Competition on the Transport of Arsenate. *J. Environ. Qual.* **1997**, *26* (4), 1133−1139.
(29) Xu, Z.; Tsang, D. C. W. Redox-Induced Transformation of Potentially Toxic Elements with Organic Carbon in Soil. *Carbon Res.* **2022**, *1* (1), 9.
(30) Yang, Q.; Bi, G.; Chen, Z.; Zeng, L.; Yang, R. Spatial Allocation of Fallow Land in Karst Rocky Desertification Areas: A Case Study in Qinglong County, Guizhou Province. *Acta Geogr. Sin.* **2018**, *73* (11), 2250−2266.
(31) Zeng, H.; Gu, S. Environmental Quality Assessment on Karst Groundwater in Antimony and Coal Mines Concentration Area of Qinglong. *Environ. Monit. China* **2017**, *33* (6), 78−86.
(32) Wang, J.; Shaheen, S. M.; Swertz, A.-C.; Rennert, T.; Feng, X.; Rinklebe, J. Sulfur-Modified Organoclay Promotes Plant Uptake and Affects Geochemical Fractionation of Mercury in a Polluted Floodplain Soil. *J. Hazard. Mater.* **2019**, *371*, 687−693.
(33) Sharma, A.; Muyskens, A.; Guinness, J.; Polizzotto, M. L.; Fuentes, M.; Tappero, R. V.; Chen-Wiegart, Y. K.; Thieme, J.; Williams, G. J.; Acerbo, A. S.; Hesterberg, D. Multi-Element Effects on Arsenate Accumulation in a Geochemical Matrix Determined Using μ-XRF, μ-XANES and Spatial Statistics. *J. Synchrotron Radiat.* **2019**, *26* (6), 1967−1979.
(34) Hemming, S. R.; Liu, T.; Northrup, P.; Nicholas, S.; Rasbury, E. T.; Chen, H.; Warden, A.; Chen, A.; Li, R.; Tappero, R.; Cox, S. E.; Everard, J.; Wang, S.; Deluca, M.; Bostick, B.; Halliday, A. N. Synchrotron Microanalytical Characterization and K/Ar Dating of the GL-O-1 Glauconite Reference Material at the Single Pellet Scale and Reassessment of the Age of Visually Mature Pellets. *Minerals* **2023**, *13* (6), 773.
(35) Yu, K.; Rinklebe, J. Advancement in Soil Microcosm Apparatus for Biogeochemical Research. *Ecol. Eng.* **2011**, *37* (12), 2071−2075.
(36) Wang, J. X.; Rinklebe, J.; Feng, X. B. Redox Transformation of Mercury in Soils. In *Methylmercury Accumulation in Rice: Process and Regulation*; Feng, X. B., Wang, J. X., Rinklebe, J., Ed.; CRC Press, 2024; pp 126−140.
(37) Ali, M. A.; Oh, J. H.; Kim, P. J. Evaluation of Silicate Iron Slag Amendment on Reducing Methane Emission from Flood Water Rice Farming. *Agric. Ecosyst. Environ.* **2008**, *128* (1), 21−26.
(38) Rinklebe, J.; Shaheen, S. M.; El-Naggar, A.; Wang, H.; Du Laing, G.; Alessi, D. S.; Sik Ok, Y. Redox-Induced Mobilization of Ag, Sb, Sn, and Tl in the Dissolved, Colloidal and Solid Phase of a Biochar-Treated and Un-Treated Mining Soil. *Environ. Int.* **2020**, *140*, No. 105754.
(39) Wang, J.; Shaheen, S. M.; Jing, M.; Anderson, C. W. N.; Swertz, A.-C.; Wang, S.-L.; Feng, X.; Rinklebe, J. Mobilization, Methylation, and Demethylation of Mercury in a Paddy Soil Under Systematic Redox Changes. *Environ. Sci. Technol.* **2021**, *55* (14), 10133−10141.
(40) Komorowicz, I.; Barałkiewicz, D. Arsenic and Its Speciation in Water Samples by High Performance Liquid Chromatography Inductively Coupled Plasma Mass Spectrometry—Last Decade Review. *Talanta* **2011**, *84* (2), 247−261.
(41) Rinklebe, J.; Shaheen, S. M.; Schröter, F.; Rennert, T. Exploiting Biogeochemical and Spectroscopic Techniques to Assess the Geochemical Distribution and Release Dynamics of Chromium and Lead in a Contaminated Floodplain Soil. *Chemosphere* **2016**, *150*, 390−397.
(42) Ravel, B.; Newville, M. ATHENA, ARTEMIS, HEPHAESTUS: Data Analysis for X-Ray Absorption Spectroscopy Using IFEFFIT. *J. Synchrotron Radiat.* **2005**, *12* (4), 537−541.
(43) Ren, G.; Zhang, H.; Lin, X.; Zhu, J.; Jia, Z. Response of Phyllosphere Bacterial Communities to Elevated CO2 during Rice Growing Season. *Appl. Microbiol. Biotechnol.* **2014**, *98* (22), 9459−9471.
(44) Russell, J. B.; Diez-Gonzalez, F. The Effects of Fermentation Acids on Bacterial Growth. In *Advances in Microbial Physiology*; Poole, R. K., Ed.; Academic Press, 1997; Vol. *39*, pp 205−234.
(45) Yan, F.; Schubert, S.; Mengel, K. Soil pH Increase Due to Biological Decarboxylation of Organic Anions. *Soil Biol. Biochem.* **1996**, *28* (4), 617−624.
(46) Manning, B. A.; Hunt, M. L.; Amrhein, C.; Yarmoff, J. A. Arsenic(III) and Arsenic(V) Reactions with Zerovalent Iron Corrosion Products. *Environ. Sci. Technol.* **2002**, *36* (24), 5455−5461.
(47) Manning, B. A.; Fendorf, S. E.; Goldberg, S. Surface Structures and Stability of Arsenic(III) on goethite: Spectroscopic Evidence for Inner-Sphere Complexes. *Environ. Sci. Technol.* **1998**, *32* (16), 2383−2388.
(48) Yokoyama, Y.; Tanaka, K.; Takahashi, Y. Differences in the Immobilization of Arsenite and Arsenate by Calcite. *Geochim. Cosmochim. Acta* **2012**, *91*, 202−219.
(49) Cui, J.; Zhao, Y.; Li, J.; Beiyuan, J.; Tsang, D. C. W.; Poon, C.; Chan, T.; Wang, W.; Li, X. Speciation, Mobilization, and Bioaccessibility of Arsenic in Geogenic Soil Profile from Hong Kong. *Environ. Pollut.* **2018**, *232*, 375−384.
(50) Wang, Y.; Jiao, J. J.; Cherry, J. A. Soils in the karst landscape Occurrence and Geochemical Behavior of Arsenic in a Coastal

Aquifer−Aquitard System of the Pearl River Delta, China. *Sci. Total Environ.* **2012**, *427*−*428*, 286−297.
(51) Dixit, S.; Hering, J. G. Comparison of Arsenic(V) and Arsenic(III) Sorption onto Iron Oxide Minerals: Implications for Arsenic Mobility. *Environ. Sci. Technol.* **2003**, *37* (18), 4182−4189.
(52) Roden, E. E.; Zachara, J. M. Microbial Reduction of Crystalline Iron(III) Oxides: Influence of Oxide Surface Area and Potential for Cell Growth. *Environ. Sci. Technol.* **1996**, *30* (5), 1618−1628.
(53) Poulton, S. W.; Krom, M. D.; Raiswell, R. A Revised Scheme for the Reactivity of Iron (Oxyhydr)Oxide Minerals towards Dissolved Sulfide. *Geochim. Cosmochim. Acta* **2004**, *68* (18), 3703−3715.
(54) Zobrist, J.; Dowdle, P. R.; Davis, J. A.; Oremland, R. S. Mobilization of Arsenite by Dissimilatory Reduction of Adsorbed Arsenate. *Environ. Sci. Technol.* **2000**, *34* (22), 4747−4753.
(55) Yee, N.; Shaw, S.; Benning, L. G.; Nguyen, T. H. The Rate of Ferrihydrite Transformation to goethite via the Fe(II) Pathway. *Am. Mineral.* **2006**, *91* (1), 92−96.
(56) Hansel, C. M.; Benner, S. G.; Neiss, J.; Dohnalkova, A.; Kukkadapu, R. K.; Fendorf, S. Secondary Mineralization Pathways Induced by Dissimilatory Iron Reduction of Ferrihydrite under Advective Flow. *Geochim. Cosmochim. Acta* **2003**, *67* (16), 2977−2992.
(57) Carlson, L.; Schwertmann, U. The Effect of CO2 and Oxidation Rate on the Formation of goethite versus Lepidocrocite from an Fe(II) System at pH 6 and 7. *Clay Miner.* **1990**, *25* (1), 65−71.
(58) Hansel, C. M.; Benner, S. G.; Fendorf, S. Competing Fe(II)-Induced Mineralization Pathways of Ferrihydrite. *Environ. Sci. Technol.* **2005**, *39* (18), 7147−7153.
(59) Yang, X.; Hinzmann, M.; Pan, H.; Wang, J.; Bolan, N.; Tsang, D. C. W.; Ok, Y. S.; Wang, S.-L.; Shaheen, S. M.; Wang, H.; Rinklebe, J. Pig Carcass-Derived Biochar Caused Contradictory Effects on Arsenic Mobilization in a Contaminated Paddy Soil under Fluctuating Controlled Redox Conditions. *J. Hazard. Mater.* **2022**, *421*, No. 126647.
(60) Huang, J.; Jones, A.; Waite, T. D.; Chen, Y.; Huang, X.; Rosso, K. M.; Kappler, A.; Mansor, M.; Tratnyek, P. G.; Zhang, H. Fe(II) Redox Chemistry in the Environment. *Chem. Rev.* **2021**, *121* (13), 8161−8233.
(61) Kocar, B. D.; Herbel, M. J.; Tufano, K. J.; Fendorf, S. Contrasting Effects of Dissimilatory Iron(III) and Arsenic(V) Reduction on Arsenic Retention and Transport. *Environ. Sci. Technol.* **2006**, *40* (21), 6715−6721.
(62) Islam, F.; Pederick, R.; Gault, A.; Adams, L.; Polya, D.; Charnock, J.; Lloyd, J. Interactions between the Fe(III)-Reducing Bacterium Geobacter Sulfurreducens and Arsenate, and Capture of the Metalloid by Biogenic Fe(II). *Appl. Environ. Microbiol.* **2005**, *71* (12), 8642−8648.
(63) Tufano, K. J.; Fendorf, S. Confounding Impacts of Iron Reduction on Arsenic Retention. *Environ. Sci. Technol.* **2008**, *42* (13), 4777−4783.
(64) Pedersen, H. D.; Postma, D.; Jakobsen, R. Release of Arsenic Associated with the Reduction and Transformation of Iron Oxides. *Geochim. Cosmochim. Acta* **2006**, *70* (16), 4116−4129.
(65) Zhang, G.; Yuan, Z.; Lei, L.; Lin, J.; Wang, X.; Wang, S.; Jia, Y. Arsenic Redistribution and Transformation during Fe(II)-Catalyzed Recrystallization of As-Adsorbed Ferrihydrite under Anaerobic Conditions. *Chem. Geol.* **2019**, *525*, 380−389.
(66) Afkar, E.; Lisak, J.; Saltikov, C.; Basu, P.; Oremland, R. S.; Stolz, J. F. The Respiratory Arsenate Reductase from Bacillus Selenitireducens Strain MLS10. *FEMS Microbiol. Lett.* **2003**, *226* (1), 107−112.
(67) Lovley, D. R. Fe(III) and Mn(IV) Reduction. In *Environmental Microbe-Metal Interactions*, 2000; pp 1−30.
(68) de Castro, A. F.; Ehrlich, H. L. Reduction of Iron Oxide Minerals by a Marine Bacillus. *Antonie van Leeuwenhoek* **1970**, *36* (1), 317−327.
(69) Arnold, R. G.; DiChristina, T. J.; Hoffmann, M. R. Reductive Dissolution of Fe(III) Oxides by Pseudomonas Sp. 200. *Biotechnol. Bioeng.* **1988**, *32* (9), 1081−1096.
(70) Mirza, B. S.; Muruganandam, S.; Meng, X.; Sorensen, D. L.; Dupont, R. R.; McLean, J. E. Arsenic(V) Reduction in Relation to Iron(III) Transformation and Molecular Characterization of the Structural and Functional Microbial Community in Sediments of a Basin-Fill Aquifer in Northern Utah. *Appl. Environ. Microbiol.* **2014**, *80* (10), 3198−3208.
(71) Langner, H. W.; Inskeep, W. P. Microbial Reduction of Arsenate in the Presence of Ferrihydrite. *Environ. Sci. Technol.* **2000**, *34* (15), 3131−3136.
(72) Stolz, J.; Ellis, D.; Blum, J.; Ahmann, D.; Lovley, D.; Oremland, R. Sulfurospirillum barnesii Sp Nov and Sulfurospirillum Arsenophilum Sp Nov., New Members of the Sulfurospirillum Clade of the ε Proteobacteria. *Int. J. Syst. Bacteriol.* **1999**, *49*, 1177−1180.
(73) Suhadolnik, M. L. S.; Salgado, A. P. C.; Scholte, L. L. S.; Bleicher, L.; Costa, P. S.; Reis, M. P.; Dias, M. F.; Ávila, M. P.; Barbosa, F. A. R.; Chartone-Souza, E.; Nascimento, A. M. A. Novel Arsenic-Transforming Bacteria and the Diversity of Their Arsenic-Related Genes and Enzymes Arising from Arsenic-Polluted Freshwater Sediment. *Sci. Rep.* **2017**, *7* (1), 11231.
(74) Shelobolina, E. S.; VanPraagh, C. G.; Lovley, D. R. Use of Ferric and Ferrous Iron Containing Minerals for Respiration by Desulfitobacterium Frappieri. *Geomicrobiol. J.* **2003**, *20* (2), 143−156.
(75) Comensoli, L.; Maillard, J.; Albini, M.; Sandoz, F.; Junier, P.; Joseph, E. Use of Bacteria To Stabilize Archaeological Iron. *Appl. Environ. Microbiol.* **2017**, *83* (9), No. e03478-16.
(76) Niggemyer, A.; Spring, S.; Stackebrandt, E.; Rosenzweig, R. Isolation and Characterization of a Novel As(V)-Reducing Bacterium:: Implications for Arsenic Mobilization and the Genus Desulfitobacterium. *Appl. Environ. Microbiol.* **2001**, *67* (12), 5568−5580.
(77) Pepi, M.; Protano, G.; Ruta, M.; Nicolardi, V.; Bernardini, E.; Focardi, S. E.; Gaggi, C. Arsenic-Resistant Pseudomonas Spp. and Bacillus Sp. Bacterial Strains Reducing As(V) to As(III), Isolated from Alps Soils, Italy. *Folia Microbiol.* **2011**, *56* (1), 29−35.
(78) Balashova, V. V.; Zavarzin, G. A. Anaerobic reduction of ferric iron by hydrogen bacteria. *Mikrobiologiia* **1979**, *48* (5), 773−778.
(79) Saltikov, C. W.; Wildman, R. A.; Newman, D. K. Expression Dynamics of Arsenic Respiration and Detoxification in Shewanella Sp. Strain ANA-3. *J. Bacteriol.* **2005**, *187* (21), 7390−7396.
(80) Malasarn, D.; Keeffe, J. R.; Newman, D. K. Characterization of the Arsenate Respiratory Reductase from Shewanella Sp. Strain ANA-3. *J. Bacteriol.* **2008**, *190* (1), 135−142.
(81) Glasser, N. R.; Oyala, P. H.; Osborne, T. H.; Santini, J. M.; Newman, D. K. Structural and Mechanistic Analysis of the Arsenate Respiratory Reductase Provides Insight into Environmental Arsenic Transformations. *Proc. Natl. Acad. Sci. U. S. A.* **2018**, *115* (37), E8614−E8623.
(82) Bahar, M. M.; Megharaj, M.; Naidu, R. Arsenic Bioremediation Potential of a New Arsenite-Oxidizing Bacterium Stenotrophomonas Sp. MM-7 Isolated from Soil. *Biodegradation* **2012**, *23* (6), 803−812.
(83) LeMonte, J. J.; Stuckey, J. W.; Sanchez, J. Z.; Tappero, R.; Rinklebe, J. R.; Sparks, D. L. Sea Level Rise Induced Arsenic Release from Historically Contaminated Coastal Soils. *Environ. Sci. Technol.* **2017**, *51* (11), 5913−5922.
(84) Buschmann, J.; Kappeler, A.; Lindauer, U.; Kistler, D.; Berg, M.; Sigg, L. Arsenite and Arsenate Binding to Dissolved Humic Acids: Influence of pH, Type of Humic Acid, and Aluminum. *Environ. Sci. Technol.* **2006**, *40* (19), 6015−6020.
(85) Mladenov, N.; Zheng, Y.; Simone, B.; Bilinski, T. M.; McKnight, D. M.; Nemergut, D.; Radloff, K. A.; Rahman, M. M.; Ahmed, K. M. Dissolved Organic Matter Quality in a Shallow Aquifer of Bangladesh: Implications for Arsenic Mobility. *Environ. Sci. Technol.* **2015**, *49* (18), 10815−10824.
(86) Burton, E. D.; Johnston, S. G.; Kraal, P.; Bush, R. T.; Claff, S. Sulfate Availability Drives Divergent Evolution of Arsenic Speciation

during Microbially Mediated Reductive Transformation of Schwertmannite. *Environ. Sci. Technol.* **2013**, *47* (5), 2221−2229.
(87) Kocar, B. D.; Fendorf, S. Thermodynamic Constraints on Reductive Reactions Influencing the Biogeochemistry of Arsenic in Soils and Sediments. *Environ. Sci. Technol.* **2009**, *43* (13), 4871−4877.
(88) Burton, E. D.; Johnston, S. G.; Kocar, B. D. Arsenic Mobility during Flooding of Contaminated Soil: The Effect of Microbial Sulfate Reduction. *Environ. Sci. Technol.* **2014**, *48* (23), 13660−13667.
(89) Rodriguez-Freire, L.; Moore, S. E.; Sierra-Alvarez, R.; Root, R. A.; Chorover, J.; Field, J. A. Arsenic Remediation by Formation of Arsenic Sulfide Minerals in a Continuous Anaerobic Bioreactor. *Biotechnol. Bioeng.* **2016**, *113* (3), 522−530.
(90) Yao, W.; Millero, F. J. Oxidation of Hydrogen Sulfide by Hydrous Fe(III) Oxides in Seawater. *Mar. Chem.* **1996**, *52* (1), 1−16.
(91) Nickson, R.; McArthur, J.; Burgess, W.; Ahmed, K. M.; Ravenscroft, P.; Rahmañn, M. Arsenic Poisoning of Bangladesh Groundwater. *Nature* **1998**, *395* (6700), 338−338.
(92) Nickson, R. T.; McArthur, J. M.; Ravenscroft, P.; Burgess, W. G.; Ahmed, K. M. Mechanism of Arsenic Release to Groundwater, Bangladesh and West Bengal. *Appl. Geochem.* **2000**, *15* (4), 403−413.
(93) Renard, F.; Putnis, C. V.; Montes-Hernandez, G.; Ruiz-Agudo, E.; Hovelmann, J.; Sarret, G. Interactions of Arsenic with Calcite Surfaces Revealed by in Situ Nanoscale Imaging. *Geochim. Cosmochim. Acta* **2015**, *159*, 61−79.
(94) Zhang, L.; Qin, X.; Tang, J.; Liu, W.; Yang, H. Review of Arsenic Geochemical Characteristics and Its Significance on Arsenic Pollution Studies in Karst Groundwater, Southwest China. *Appl. Geochem.* **2017**, *77*, 80−88.
(95) Jiku, M. A. S.; Zeng, X.; Li, L.; Li, L.; Zhang, Y.; Huo, L.; Shan, H.; Zhang, Y.; Wu, C.; Su, S. Soil Ridge Cultivation Maintains Grain As and Cd at Low Levels and Inhibits As Methylation by Changing arsM-Harboring Bacterial Communities in Paddy Soils. *J. Hazard. Mater.* **2022**, *429*, No. 128325.
(96) Connolly, S.; O'Flaherty, V.; Krol, D. J. Inhibition of Methane Production in Cattle Slurry Using an Oxygen-Based Amendment. *J. Cleaner Prod.* **2023**, *394*, No. 136272.

https://doi.org/10.1021/acs.est.4c02989
Environ. Sci. Technol. 2024, 58, 17850−17861